© 2020. Published by The Company of Biologists Ltd | Journal of Experimental Biology (2020) 223, jeb219873. doi:10.1242/jeb.219873

RESEARCH ARTICLE

Morphology, performance and fluid dynamics of the crayfish escape response

Jocelyn Hunyadi[1,*,‡], Todd Currier[2,‡], Yahya Modarres-Sadeghi[2], Brooke E. Flammang[3] and Ethan D. Clotfelter[§]

ABSTRACT

Sexual selection can result in an exaggerated morphology that constrains locomotor performance. We studied the relationship between morphology and the tail-flip escape response in male and female rusty crayfish (*Faxonius rusticus*), a species in which males have enlarged claws (chelae). We found that females had wider abdomens and longer uropods (terminal appendage of the tail fan) than males, while males possessed deeper abdomens and larger chelae, relative to total length. Chelae size was negatively associated with escape velocity, whereas longer abdomens and uropods were positively associated with escape velocity. We found no sex-specific differences in maximum force generated during the tail flip, but uropod length was strongly, positively correlated with tail-flip force in males. Particle image velocimetry (PIV) revealed that the formation of a vortex, rather than the expulsion of fluid between two closing body surfaces, generates propulsion in rusty crayfish. PIV also revealed that the pleopods (ventral abdominal appendages) contribute to the momentum generated by the tail. To our knowledge, this is the first confirmation of vortex formation in a decapod crustacean.

KEY WORDS: Chelae, Escape velocity, Particle image velocimetry, Vortex

INTRODUCTION

Animal performance is the ability to accomplish ecologically relevant tasks, such as foraging and predator avoidance, and is the result of the integration of morphological, physiological and behavioral traits (Irschick and Garland, 2001; Irschick et al., 2008). Sexual selection may exaggerate morphological traits used for locomotion, and this exaggeration may reduce animal performance or increase energetic costs. However, previous studies of the effects of sexual selection on performance have yielded conflicting results (Cameron et al., 2013; Tullis and Straube, 2017; Kojima and Lin, 2018). One potential explanation for this ambiguity is that compensatory strategies or structures may evolve to offset these locomotor costs (Oufiero and Garland, 2007; Husak and Swallow, 2011). Examples of such compensatory mechanisms include longer hindlimbs to offset the weight of larger heads in female geckos (Cameron et al., 2013), larger wings to decrease the moment of inertia in male stalk-eyed flies (Husak et al., 2011) and longer supporting legs in species of fiddler crabs with larger claws or lateral claw-waving displays (Bywater et al., 2018).

Decapod crustaceans have appendages that have been modified heavily by sexual selection. Much work has focused on the sexually dimorphic major claws (chelae) of lobster (*Homarus americanus*: Elner and Campbell, 1981), fiddler crabs (*Uca pugnax*: Levinton and Judge, 1993), hermit crabs (*Pagurus nigrofascia*: Yasuda et al., 2011) and crayfish [*Faxonius* (=*Orconectes*) *propinquus*: Stein, 1976; *Procambarus clarkii*: Malavé et al., 2018]. Among crayfish, for example, chelae are important determinants of reproductive success. Chelae are required to manipulate the female during mating, and chelae size is associated with male mating success (Stein, 1976; Sneddon, 1990). During male–male competition, the physical strength of the opponent is often assessed via chelae size (Wilson et al., 2007). Such signals, however, may be dishonest indicators of strength (Wilson et al., 2007; Walter et al., 2011) and thus are frequently tested during agonistic encounters. Body size, chelae size and chelae morphology all influence the outcome of contests, and therefore ultimately affect dominance hierarchies (Walter et al., 2011; Ueno and Nagayama, 2012) and access to resources and mates (Herberholz et al., 2007; Aquiloni et al., 2008). However, large chelae impose significant metabolic costs (Tullis and Straube, 2017) and are known to reduce locomotor performance (Wilson et al., 2009).

One of the best-characterized forms of locomotion in decapod crustaceans is a stereotyped escape response called the tail flip. This locomotor behavior involves rapid abdominal flexion to produce powerful swimming strokes that can propel the animal away from a threat. The tail flip is an excellent system in which to examine the effects of sexual selection on performance. The kinematics and overall performance of the tail flip have been examined in numerous species, including lobsters (*H. americanus*: Cromarty et al., 1991; *Panulirus interruptus*: Nauen and Shadwick, 1999), shrimp (*Crangon crangon*: Arnott et al., 1998) and crayfish (*Faxonius virilis*: Webb, 1979; *Cherax dispar*: Wilson et al., 2009). Furthermore, there is extensive literature on the neural mechanisms underlying this escape response (e.g. Kennedy and Takeda, 1965; Wine and Krasne, 1972). In crayfish, there are three types of tail-flip escape responses mediated by different axons: lateral giant (LG), medial giant (MG) and non-giant (NG) (Wine and Krasne, 1972). In the LG tail flip, the crayfish pitches forward and upward, away from a stimulus applied to the posterior end. By contrast, the MG and NG axons fire in response to an anterior stimulus and result in the crayfish moving posteriorly, away from the stimulus.

Less is known about the fluid dynamics of the tail-flip escape response. Daniel and Meyhöfer (1989) proposed a ‘squeeze force’ model for the common dock shrimp (*Pandalus danae*), in which a fluid jet is the result of force produced as two surfaces – the tail and ventral surface of the abdomen – close against one another. If squeeze

[1]Department of Biology, Amherst College, Amherst, MA 01002, USA. [2]Department of Mechanical and Industrial Engineering, University of Massachusetts, Amherst, MA 01003, USA. [3]Federated Department of Biological Sciences, New Jersey Institute of Technology, Newark, NJ 07102, USA.
*Present address: Department of Epidemiology and Biostatistics, Texas A&M University, College Station, TX 77843, USA.
‡These authors contributed equally to this work

§Author for correspondence (edclotfelter@amherst.edu)

B.E.F., 0000-0003-0049-965X; E.D.C., 0000-0002-6711-3873

Received 9 December 2019; Accepted 12 June 2020

Journal of Experimental Biology (2020) 223, jeb219873. doi:10.1242/jeb.219873

forces were primarily responsible for the propulsion necessary to overcome drag, then maximum forces should be observed approximately as the tail closes against the abdomen. However, in their study on the California spiny lobster (*P. interruptus*), Nauen and Shadwick (2001) found that maximum forces were achieved before the tail contacted the abdomen. This result suggests either that jet formation via squeeze forces plays very little or no role in generating the total propulsive force or that different propulsive mechanisms are important in species of different body sizes.

In the current study, we investigated the relationship among sexual dimorphism, locomotor performance and fluid dynamics in the rusty crayfish *Faxonius* (=*Orconectes*) *rusticus* (Girard 1852). Outcomes of contests between *F. rusticus* males, similar to those in other species, are influenced by male size and behavior, and thus sexual selection acts strongly on males (Sneddon, 1990). Males are also subject to strong natural selection on the escape response; they wander extensively during the breeding season and are exposed to high rates of predation (Berrill and Arsenault, 1982; 1984). The first goal of our study was to identify sexual dimorphism in the chelae, abdomen and tail (including the uropods and telson that make up the tail fan) that may be relevant to locomotion, as has been reported for other decapods (Nauen and Shadwick, 1999; Wang et al., 2011). Second, we quantified three measures of tail-flip performance – maximum velocity, acceleration and force – and compared these between males and females. Third, we sought to test whether sexual selection on chelae size imposes a trade-off in terms of reduced tail-flip performance, which has previously been demonstrated in other crayfish (Wilson et al., 2009). We also examined the role of other morphological traits in predicting performance to evaluate whether male rusty crayfish have morphological adaptations (e.g. abdomen or tail fan) that may compensate for their enlarged chelae, as was reported for fiddler crabs (Bywater et al., 2018). Fourth and lastly, we characterized fluid motion around the tail during the tail-flip escape response (Nauen and Shadwick, 1999; Lim and DeMont, 2009) and confirmed the mechanism for vortex formation, as opposed to squeeze forces, in the tail-flip response in rusty crayfish.

MATERIALS AND METHODS

Study organism

We obtained rusty crayfish from a commercial supplier (Connecticut Valley Biological Supply, Southampton, MA, USA). Upon arrival, crayfish were allowed to acclimate to the laboratory for at least 24 h. Males and females were housed in separate plastic tubs (approximately 38×45 cm) with 5–7 cm of aged tap water. Tubs contained clay flower pots and sections of PVC pipe for shelter, and a pump with an air stone to ensure adequate oxygenation. Crayfish were maintained on a 14 h:10 h light:dark cycle (with 30 min of dim light to simulate dawn and dusk) and fed algae wafers daily.

Morphometrics

After cooling crayfish in ice water to slow movement, 81 (43 males and 38 females) were measured. Total body length and the length and width of the chelae, abdomen, uropods and telson were measured to ±0.1 mm with digital calipers (Fig. 1).

Tail-flip velocity

Typewriter-correction fluid (WiteOut®) was used to apply a white dot to the left side of the carapace prior to filming. Crayfish were placed individually on a submerged platform within a 38 l glass aquarium, and positioned such that their antennae were between two electrodes and the tail was at the platform edge. A Grass SD9 Stimulator was used to apply a shock of 7 V. Shocks of similar magnitude (6 V) were used in a previous study to elicit tail-flip responses in the California spiny lobster (*P. interruptus*) (Nauen and Shadwick, 1999). The tank was illuminated with two banks of 216 LED lights (14 W, 5400 k), and a video camera (Casio EX-ZR850; 240 frames s^{-1}) recorded tail-flip escape responses.

Crayfish were induced to tail flip 3 times before being removed and replaced with another subject. We excluded from our analysis any videos in which the crayfish broke the surface of the water or contacted the walls or corners of the testing tank. Therefore, only tail flips that propelled the crayfish in the positive *y*-direction (Fig. S1) and did not obscure the white tracking dot on the side of the carapace were included. If none of the three tail flips met these criteria, the process was repeated 24–48 h later. For each of the 66 crayfish used (34 males and 32 females), we used the maximum velocity for our analysis to avoid performance decline due to exhaustion. A trajectory for each tail flip was then extracted using the trajR package in R (McLean and Volponi, 2018) and used to obtain the maximum escape velocity and maximum acceleration.

Tail-flip force

The force generated during the tail-flip escape response was obtained for 10 male and 6 female crayfish across a range of body

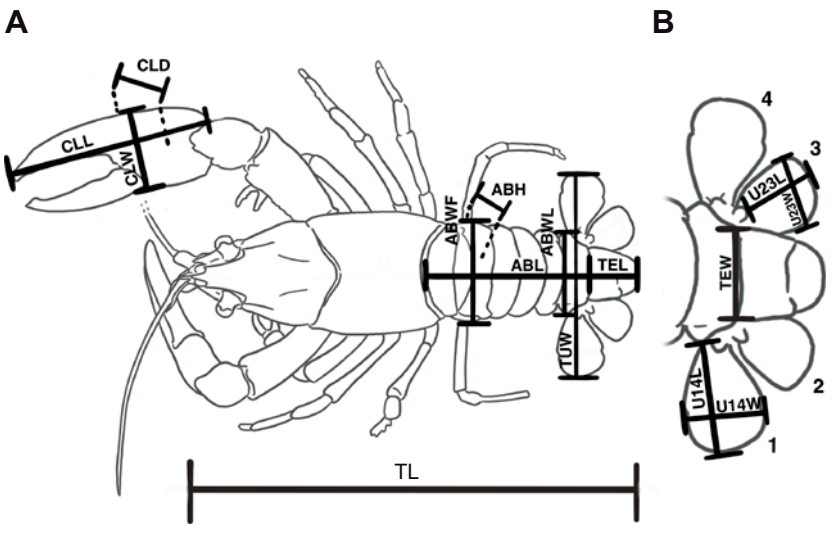

Fig. 1. Measurements taken from rusty crayfish. (A) Body measurements. (B) Tail measurements. ABL, abdominal length; ABH; abdominal height at first segment; ABWF, first abdominal segment width; ABWL, last abdominal segment width; CLD, chelae depth; CLL, chelae length; CLW, chelae width; TEL, telson length; TEW, telson width; TL, total length; TUW, total uropod width; U*xx*L, uropod length; U*xx*W, uropod width. Uropods were numbered 1–4 as indicated.

Journal of Experimental Biology (2020) 223, jeb219873. doi:10.1242/jeb.219873

sizes. Each individual was fitted with a 3D-printed mount, which was attached to the carapace with Loctite Super Glue™ and marine epoxy. The mount was connected to a Nano17 six-axis load cell (ATI Industrial Automation) via a metal rod (Fig. 2). We recorded force data in two dimensions (F_x and F_y) at a frequency of 1 kHz (Fig. 2), averaging every 10th sample. The load cell was calibrated by measuring the force recorded in each dimension with 20 and 100 g weights. The crayfish was suspended on its side in the middle of a 55×43×152 cm aquarium (Fig. 2). As before, a shock of 7 V from a Grass SD9 Stimulator was used to induce tail flips. Each crayfish was induced to tail flip 5 times before being replaced by another individual, and the maximum force value was used in subsequent analysis. Force was recorded for 15 s; the shock was administered 1–2 s after the load cell started recording. As soon as we observed a tail flip, the camera was triggered to record for 2 s at 1000 frames s^{-1} and at an exposure rate of 1 ms; the camera recorded 750 ms before and 1250 ms after being triggered. Maximum total force was calculated by taking the root mean square (RMS) of the F_x and F_y components. F_x and F_y correspond to the *x*- and *y*-positional components used to extract velocity and acceleration values (Fig. S1).

Particle image velocimetry

To visualize the movement of water around crayfish during a tail flip, we used both planar (2D) and volumetric (3D) particle image velocimetry (PIV). For 2D PIV, two male and one female crayfish were fitted with 3D-printed mounts and suspended from a metal rod in a 38 l aquarium, using the same apparatus as in Fig. 2. This allowed us to isolate the fluid dynamics produced by the tail while minimizing movement of the chelae. The aquarium was seeded with 50 µm hollow glass spheres (Dantec Dynamics PSP-50, Skovlunde, Denmark). A Phantom Miro M110 camera, set to 600 frames s^{-1}, was positioned directly below the aquarium. Three green sheet lasers (0.5 W, 532 nm) were used to illuminate the midplane of the crayfish, two of which were positioned facing the ventral surface and the third facing the posterior end. Similar to previous experiments, electrodes delivered a 7 V shock to stimulate the tail-flip escape response. PIV analysis was conducted via PIVview2C software (PIVTEC 2018). The field was interrogated using a multi-pass standard (FFT) correlation, which allowed eight passes with sub-pixel image shifting. A 32×32 pixel window, with 75% overlap per pass, was used. A third-order B-spline interpolation was used on all passes. Data were post-processed by applying a median filter with a kernel size of 3×3. Planar PIV results were obtained for three crayfish (two males and one female) and thus no statistical analysis was performed.

For 3D PIV experiments, 6 male and 6 female crayfish were similarly attached to 3D-printed mounts, which were fitted to a rod hung above a 2650 l flow tank. Neutrally buoyant 50 µm particles within the volume of interest were illuminated by a 100 mJ Nd:YAG dual-head pulse laser, pulsed at a frequency of 50 Hz. The tank was stirred between individual experimental trials to keep particles in suspension, but data were gathered while flow was turned off so that vorticity would not be shed artificially. Again, electrodes delivered a 7 V shock to stimulate the tail-flip escape response. Approximately 4–5 sequences, 2 s in duration, were collected for each individual, resulting in 57 sequences total, each with multiple tail flips. The V3V camera system has three independent lenses and CCD arrays (2048×2048 pixels) that face the lateral aspect of the flume working section. The system was calibrated by traversing a known target across the transverse (*Z*) plane of the flow tank, in the volume and downstream of where the crayfish were located. Groups of image pairs (one pair per camera, three pairs total) were captured at 50 Hz with 1.2 ms between each image pair, at 12-bit resolution. The volume imaged was 14×14×12 cm, and for each image pair approximately 80,000 particles were identified in all three images, and from these approximately 40,000 triplets representing three views of the same particle were identified and tracked between laser pulses. These particles were gridded to give a final volumetric matrix of 57×57×48 vectors (i.e. 155,952 total vectors within the volume). The resulting vector files were imported into Tecplot 360 (Tecplot, Inc., Bellevue, WA, USA) to reconstruct 3D fluid structures for analysis. Vortical isosurfaces were defined using vorticity magnitude and colored by *x*-component vorticity (parallel to the *x*-axis, describing rotation rate in the *y*–*z* plane).

Statistical analyses

We performed statistical analyses in R-Studio Version 1.0.153 (http://www.R-project.org/). Male crayfish were generally larger than females, so to control for differences in overall body size, we divided the linear dimensions of all structures by total crayfish

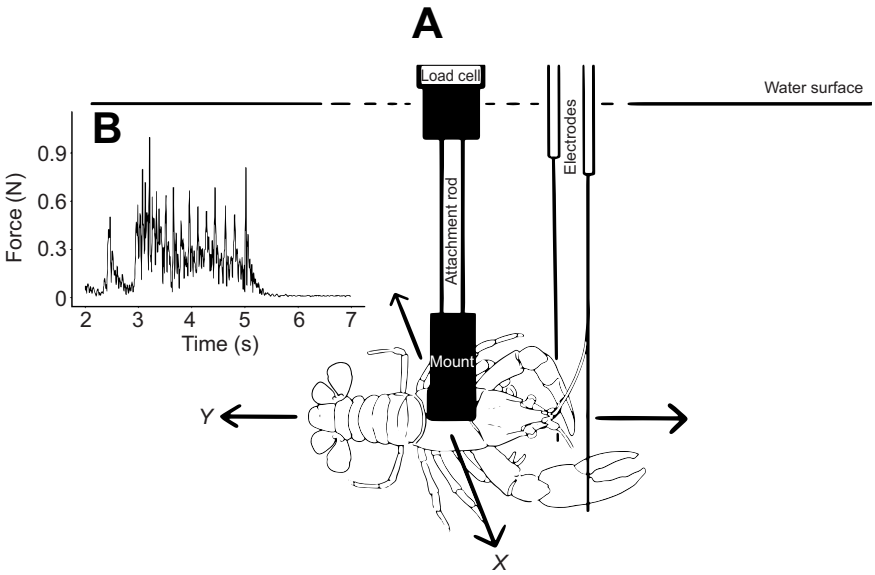

Fig. 2. Schematic diagram of the apparatus used to measure tail-flip force in rusty crayfish. (A) Crayfish suspended by the load cell during a trial. (B) Representative time-series force data from an individual crayfish. The load cell collected data on force generated along the *x*-axis (dorsal–ventral) and *y*-axis (anterior–posterior).

Journal of Experimental Biology (2020) 223, jeb219873. doi:10.1242/jeb.219873

length. Because the resulting values were not normally distributed, we used Wilcoxon rank-sum tests to evaluate sexual dimorphism. Because of the large number of morphological comparisons, the false-discovery rate (FDR) correction was applied to all *P*-values using the 'p.adjust' function. Similarly, we used a Wilcoxon rank-sum test to assess differences in maximum escape velocity and maximum escape acceleration between males and females.

Principal component analysis (PCA) was applied to the morphological measurements. The first four principal components explained approximately 90% of the variation in morphology. However, the results of PCAs were not included here because the principal components were not better predictors of escape performance than the raw data.

Prior to fitting linear regression models, the relationship between maximum escape velocity and each morphological variable was assessed for linearity. To test for a relationship between morphological variables and maximum escape velocity we used simple linear regression (SLR) models, with *P*-values corrected using the FDR method to reduce the risk of Type I errors. Multiple linear regression models were also fitted and final models selected via backward selection from the pool of variables identified as significant in SLR models. The same statistical procedure was followed with acceleration as the response variable. The morphological variables measured were also assessed for their significance in predicting maximum total force by fitting SLR models. Best-fit regression models were determined by comparing Akaike's information criterion (AIC) values. A permutation test with 10,000 iterations was applied to address the sensitivity of the multiple regression model to normality assumptions. Male and female velocity and vorticity in the PIV analysis were compared with a *t*-test.

RESULTS

Morphology

We quantified sexual dimorphism in 81 crayfish (43 males and 38 females; Fig. S2). Males were longer ($P<0.001$) and weighed more ($P<0.001$) than females. All linear dimensions we report below were adjusted for size by dividing by total length. Males had significantly longer ($P<0.001$), wider ($P<0.001$) and deeper ($P<0.001$) chelae compared with females, whereas females had wider abdomens than males at the first ($P<0.001$) and last ($P<0.001$) segments. Males, however, had greater abdominal height ($P<0.001$) than females. Females had longer ($P=0.001$) and wider ($P=0.001$) uropods than males, though the absolute differences in these structures were small. Even after applying the FDR correction, the observed differences remained significant at $P<0.05$ (Fig. S2).

Tail-flip performance

We obtained data on maximum escape velocity and acceleration for 66 free-swimming crayfish (34 male and 32 female). Total length and body mass were not significant predictors of maximum escape velocity and acceleration (Fig. S3). Values for maximum escape velocity ranged from 16.36 to 67.6 cm s^{-1}, with a mean of 39.65 cm s^{-1} and standard deviation of 9.7 cm s^{-1} (hereafter, values are reported as means±s.d.). There was a trend for females to reach higher velocities than males, but this difference was not significant (males: 37.89±8.72 cm s^{-1}; females: 42.19±10.6 cm s^{-1}; $t=1.67$, $P=0.10$).

We found three morphological traits to be significant predictors of maximum escape velocity: abdomen length (β=163.83, $P=0.046$, AIC=451.04), chelae depth (β=−162.74, $P=0.035$, AIC=443.83) and inner uropod length (β=438.89, $P=0.005$, AIC=446.85) (Fig. 3). Although not significant, models fitted with chelae length (β=−29.66, $P=0.055$, AIC=444.63) or chelae width (β=−91.09, $P=0.52$, AIC=444.53) as the sole predictor had low AIC values. The best multiple regression model included abdomen length, inner uropod length, chelae length and chelae depth as predictors (AIC=439.04), although chelae length and chelae depth were not significant ($P>0.05$).

Values for maximum escape acceleration ranged from 1161 to 6197 cm s^{-2}, with a mean of 2246±712 cm s^{-2}. Females reached higher maximum acceleration than males (males: 2050±471 cm s^{-2}; females: 2530±896 cm s^{-2}; $t=2.45$, $P=0.019$). Five morphological variables (all divided by total length) were significant predictors of maximum escape acceleration: first abdominal segment width (β=13,207, $P=0.039$, AIC=975.01), chelae length (β=−3016, $P=0.007$, AIC=956.81), chelae width (β=−9237, $P=0.007$, AIC=956.66), chelae depth (β=−15,697.3, $P=0.005$, AIC=956.17) and inner uropod length (β=37,128, $P=0.001$, AIC=968.13) (Fig. 3). The best multiple regression model included inner uropod length and chelae length as predictors (AIC=953.74), although chelae length was not significant ($P>0.05$).

Tail-flip force

For 16 crayfish (10 males and 6 females) constrained in the apparatus shown in Fig. 2, maximum total force during the tail flip ranged from 0.43 to 1.2 N. Total length and body mass were not significant predictors of the total maximum force generated (Fig. S4). None of the morphological traits were significant predictors of tail-flip force, but a model including the interaction between crayfish sex and the size-adjusted length of the inner uropod was significant (inner uropod length: β=−3.196, $P=0.74$; sex: β=−5.83, $P=0.022$; interaction: β=55.98, $P=0.02$; AIC=2.24). Furthermore, when only male crayfish were considered, inner uropod length was a significant predictor of maximum force (β=52.79, $P<0.004$, AIC=−4.7; Fig. S5).

The generation of force in the *x*-plane (F_x) corresponds to movement along the dorsal–ventral plane (Fig. 2; Fig. S1). None of the morphological traits were significantly correlated with maximum F_x. However, the relationship between uropod size and maximum F_x differed between males and females. Inner uropod length was a stronger predictor of maximum F_x in males than in females (inner uropod length: β=0.18, $P=0.97$; sex(male): β=−2.83, $P<0.018$; interaction: β=28.18, $P=0.014$; AIC=−21.95; Fig. 4A). To address the sensitivity of the multiple regression model to normality assumptions, we carried out a permutation procedure where the interaction term was shuffled 10,000 times. This procedure yielded a *P*-value of 0.0145, similar to that of the parametric model. When only males were considered, a model with relative inner uropod length accounted for 48% of the variability in maximum F_x (AIC=−12.13). Similarly, a model with outer uropod length accounted for 40% of the variability (AIC=−10.56). For females, there was no significant relationship identified between inner or outer uropod length and maximum F_x.

The generation of force in the *y*-plane (F_y) corresponds to movement along the anterior–posterior plane (Fig. S1). Outer uropod length was significantly, positively correlated with maximum F_y (β=27.06, $P=0.005$, AIC=4.23), while inner uropod length was not quite statistically significant (β=16.57, $P=0.056$, AIC=9.40; Fig. 4B). When considering only males, outer and inner uropod length was more strongly associated with maximum F_y. Outer and inner uropod length accounted for 42% (AIC=1.33) and 54% (AIC=−0.96) of the variation in maximum F_y, respectively. When only females were considered, there was no significant relationship observed between outer or inner uropod length and maximum F_y. Estimated slope coefficients, however, were positive, similar to findings in males.

Journal of Experimental Biology (2020) 223, jeb219873. doi:10.1242/jeb.219873

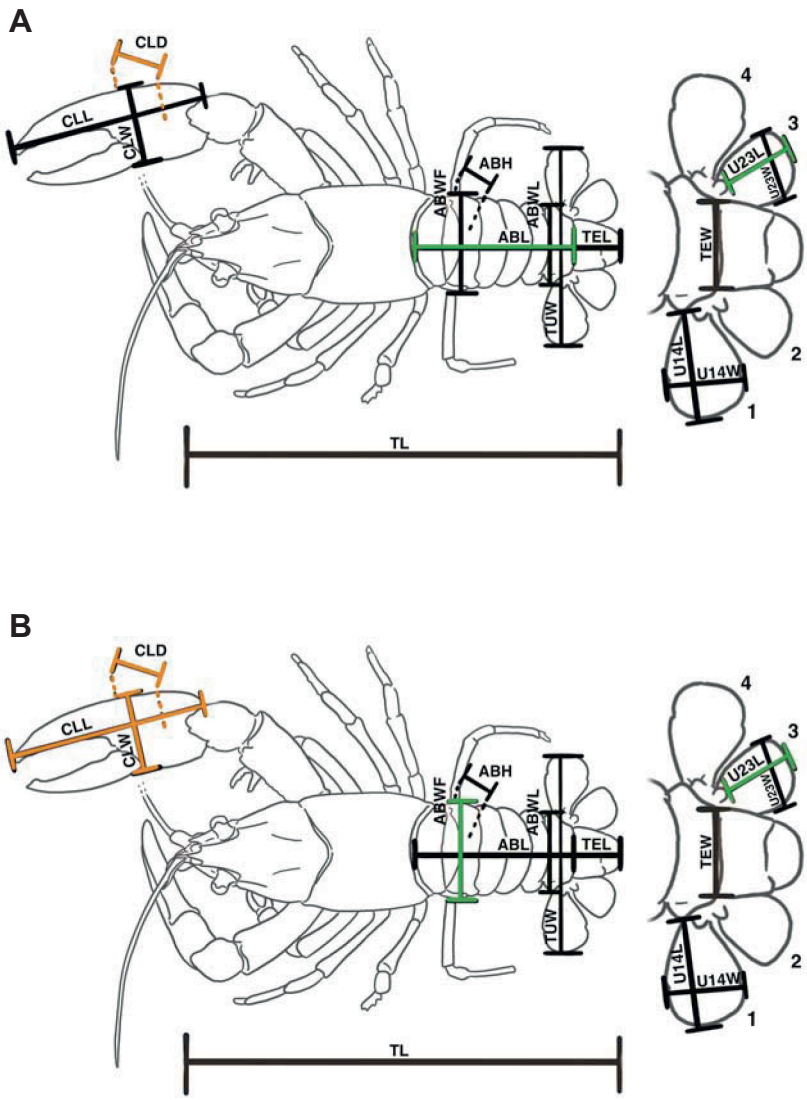

Fig. 3. Morphological predictors of escape performance in rusty crayfish. In A and B, the full body is shown on the left, and the enlarged tail fan on the right; see Fig. 1 for a complete list of structures. (A) Size-adjusted ABL and U23L were positively associated with maximum escape velocity (green) while size-adjusted CLD was negatively associated with maximum escape velocity (orange). The best multiple linear regression model included ABL and U23L. (B) Size-adjusted ABWF and U23L were positively associated with maximum escape acceleration (green) while size-adjusted CLD, CLL and CLW were negatively associated with maximum escape acceleration (orange).

Kinematics, kinetics and fluid dynamics of the tail flip

A tail-flip escape response was initiated with rapid dorsal elevation of the walking legs and straightening of the abdomen along the long axis (Movie 1). Caudally, the telson and uropods spread laterally and rotate to a ventrally angled position, forming a cupped shape. Metachronal motion of the ventral abdominal appendages (pleopods or swimmerets; Fig. 5, yellow arrows) occurred for 0.20±0.08 s before tail-flip actuation. The tail flip itself was performed in approximately 0.02–0.04 s, and was followed either by a rest period with the tail pressed ventrally against the abdomen, or the tail was immediately extended to initiate a sequential round of pleopod paddling and another tail flip.

Prior to the initiation of the tail-flip response, the crayfish were observed to display a periodic motion of their pleopods. This behavior was observed in both males and females. The motion was characterized by two distinct stages: (i) the upstroke and (ii) the downstroke. During the upstroke, all pleopods were drawn simultaneously to the abdomen. In this stage, the pleopods were curved and deformed as a result of the fluid drag. During the downstroke, the pleopods were less curved and followed a metachronal motion, starting with the set closest to the tail (Fig. 6A). The upstroke took on average 0.17±0.03 s to complete, while the downstroke took 0.29±0.02 s.

The implication of this steady pleopod paddling was that the fluid surrounding the abdomen of the crayfish was entrained and directed toward the tail. The fluid flow was then redirected by the cupped tail, producing a vortex ring (Fig. 6B). In the planar PIV, the vortex ring appears as two counter-rotating vortices: the one on the upper side of the tail rotates in the clockwise (CW) direction, and the one on the lower side rotates in the counterclockwise (CCW) direction. As shown in Fig. 7, the direction of rotation of the upper vortex (CW) is the same as the direction of rotation of the vortex that is created during the tail flip. Intermittent movements of the tail and abdomen were observed to cause the vortex to shed in the wake, resulting in vortex pairs that were observed downstream of the animal (Fig. 6C). The steady pleopod paddling generated forces an order of magnitude smaller than the peak forces generated during the tail-flip response (Fig. 6D).

The steady pleopod paddling was then followed by tail flips. Sample time histories of the flow forces acting on the specimen during the maneuver are depicted in Fig. 7A. The steady-state swimming can be observed at the start and the end of the sample time history, as the relatively small-magnitude oscillations for t=0–0.15 s and t=2.5–2.9 s. In the selected time history, this crayfish performed 14 tail flips in rapid succession. The average time between peaks was 0.164±0.0195 s (±95% confidence interval).

Journal of Experimental Biology (2020) 223, jeb219873. doi:10.1242/jeb.219873

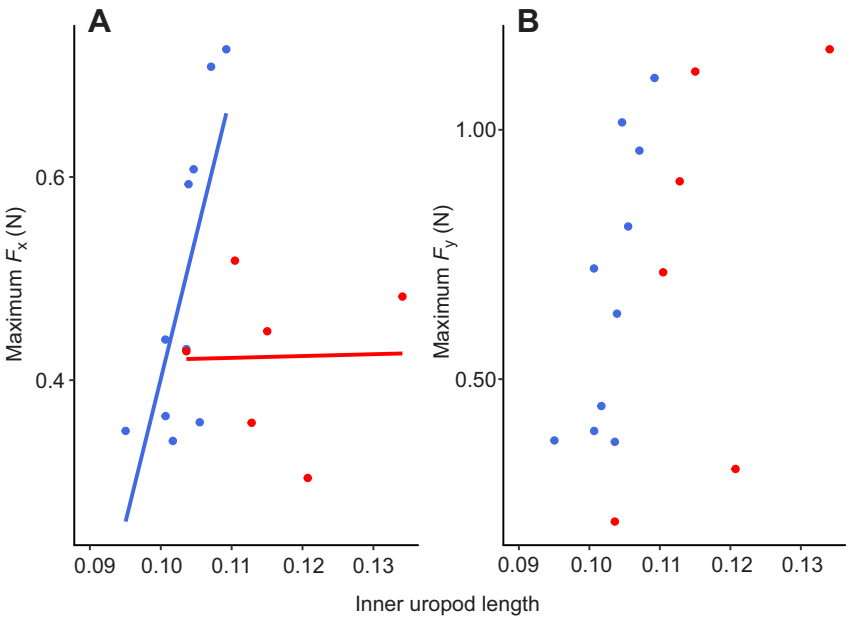

Fig. 4. Relationship between uropod length and force production in rusty crayfish. Uropod length was adjusted by total body length; F_x (*x*-force) and F_y (*y*-force) are the forces generated in the dorsal–ventral and anterior–posterior planes, respectively, during the tail flip escape response. (A) Inner uropod length (U23L) was significantly related to maximum *x*-force in males, but not in females (P=0.014). (B) Inner uropod length (U23L) was weakly related to maximum *y*-force (P=0.056). The correlation between uropod length and maximum *y*-force remained significant (A) even with moderately influential and high leverage points removed. Blue, males; red, females.

The mean peak value of force in the direction of anticipated escape (negative *y*-direction) was 0.421±0.025 N. Here, we focus on a single tail flip transient, immediately following the steady swimming condition up until the first peak force was observed (Fig. 7B). The tail flip initiation point, shown in Fig. 7B, was identified from the video data as the first observable motion of the tail. It is important to note that after the peak force was observed, the motion of the animal was constrained by the mount, and therefore the resulting measured force and observed hydrodynamics deviate from those of a free-moving animal. Fig. 7C shows the location of the mount, and the orientation of the F_x and F_y forces that were measured. The test apparatus was designed to be adequately stiff to constrain the crayfish, but at the same time allowed for small measurable deformation under loading. This deformation permitted the animal to move in its intended direction until the maximum force was reached, which can be seen in the sudden change in the slope of the measured force at t≈0.22 s in Fig. 7B. The potential energy stored in the mount due to its deformation is then released, which causes a decaying oscillatory motion, not attributed to the unconstrained behavior of the animal. These oscillations, which can be easily identified in the time histories, were used to synchronize the force measurements and the PIV results. The displacement of the mount point on the animal was tracked simultaneously with the image velocimetry calculations. The phase of the oscillatory displacement attributed to the test setup vibration (20.08 Hz) was aligned to be 180 deg out of phase with independently measured forces.

In Fig. 7C we show the crayfish at the end of its tail-flip response, where evidence of a large vortex can be observed. This vortex is formed during the tail flip and is shed at the end of the tail flip. The vortex generated during the tail flip was more clearly observed using planar PIV techniques. Sample PIV results are shown in Fig. 7D for three instances during the tail-flip maneuver: (i) 0.01 s after initiation, (ii) 0.02 s after initiation and (iii) at the point corresponding to the peak force. These points are also highlighted in Fig. 7B. Movie 2 shows the development of the flow field over a single tail flip response. As the tail flip starts and the tail moves downward, a vortex begins to be formed and also results in accelerating the mass of fluid immediately in contact with it (Fig. 7Di). The vortex rotates in the clockwise direction, the same direction as the direction of rotation of the vortex that was created at the upper side of the tail during steady-state swimming due to the movements of the pleopods. This vortex becomes larger as the tail bends more (Fig. 7Dii) and when the tail stops at the end of the tail flip response, the vortex is shed (Fig. 7Diii). When the vortex is shed, it applies a force in the opposite direction of shedding (i.e. toward the tail) on the animal. The wake shown in Fig. 7Diii is at the instant of peak measured force in Fig. 7B.

Qualitative 3D visualization provided evidence to suggest that the out-of-plane aspects of the flow could also play a role in the escape response, and for this reason volumetric flow analyses (3D PIV)

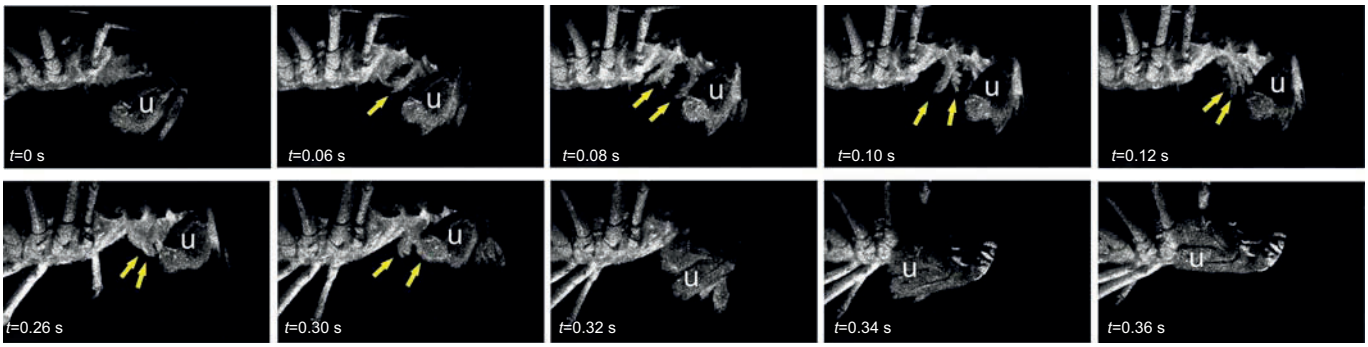

Fig. 5. Video frames of a crayfish tail flip captured during volumetric (3D) particle image velocimetry (PIV). Time zero is designated as the beginning of abdominal straightening. Pleopods (swimmerets) are designated by yellow arrows; U represents the left outer uropod.

Journal of Experimental Biology (2020) 223, jeb219873. doi:10.1242/jeb.219873

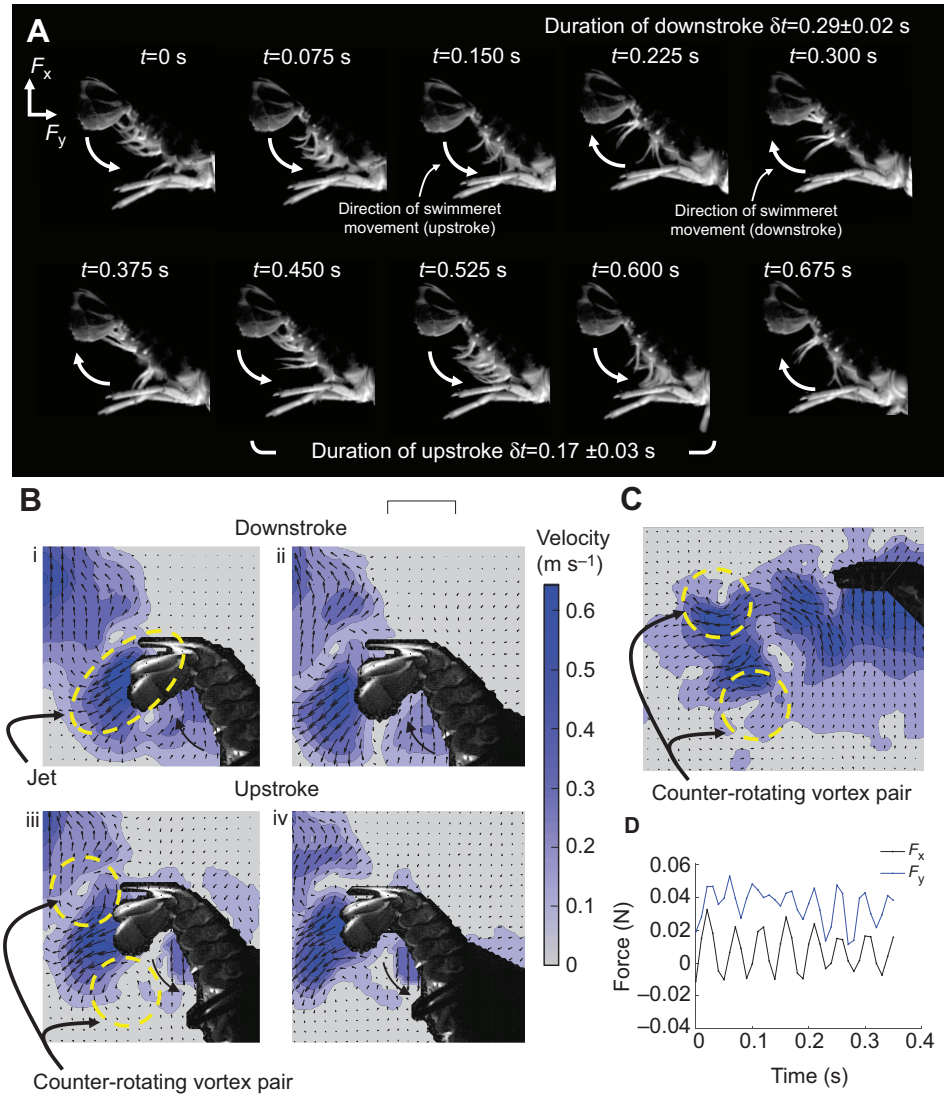

Fig. 6. Pleopod steady-state movement and formation of a jet by the crayfish tail. (A) A series of images showing the steady movement of the pleopods, before the initiation of the tail flip. The periodic movement of the appendages is shown to create a fluid flow underneath the body, which then interacts with the tail, and produces two counter-rotating vortices in the wake (B). The two vortices remain close to the tail until the tail moves a bit, which then results in the shedding of those two vortices into the wake (C). The shedding of these vortices then creates a reaction force on the crayfish in the direction of the head. (D) The repetitive movement of the tail results in a sinusoidal force on the crayfish in both the *x*- and *y*-directions.

were performed. The 3D PIV revealed that the flow observed at the mid-plane produced by the metachronal paddling of the pleopods produced vortices (Fig. 8A), which were pushed posteriorly along the ventral abdomen towards the cupped tail. The tail flip generated a single vortex oriented antero-ventrally at an angle of approximately 35–45 deg from the main axis of the body (Fig. 8B). This anteriorly directed vortex produced by the tail flip passed ventral to the posteriorly directed vortices generated by the pleopods. Male crayfish produced a significantly higher average maximum velocity during tail flip (2.65±0.30 m s^{-1}; t_{49}=1.67, P=0.013) than did female crayfish (2.42±0.37 m s^{-1}). However, there was no significant difference in average maximum vorticity between male and female tail flips (0.96±0.17 s^{-1} and 0.94±0.11 s^{-1}, respectively; P=0.27). In addition to momentum augmentation by the pleopods, it was observed that the rapid dorsal elevation of the walking legs could generate vortices; these vortices were more lateral to the abdomen but appeared to also become entrained within the cupped uropods (Fig. 8C).

In Fig. 9 we provide an illustration of the hydrodynamics based on the results of the planar and 3D PIV. Fig. 9A shows the flow field during the steady pleopod paddling condition. The fluid is entrained by the pleopods and directed toward the tail. The cupped tail subsequently directs the fluid to exit parallel to the telson. The exiting flow interacts with the surrounding still fluid to produce a vortex ring. The planar PIV results indicate that this ring remains attached to the tail (Fig. 6B) of the animal, and it is shed by intermittent larger tail movements (Fig. 6C).

In Fig. 9B an illustration of the hydrodynamics associated with the tail flip is depicted. The results shown in the 3D PIV and the visualization in Movie 3 indicate that the tail flip results in a horseshoe-shaped vortex. The reason for this can be understood as a combination of tail geometry and tail-flip kinematics. Fig. 9Bi shows the overall architecture of the flow, where a mass of fluid is accelerated by the surface of the tail and results in a vortex with greater vorticity at the tip of the tail as compared to the tail–body connection. The fluid mass and vortex are driven to follow the trajectory of the tail and result in the breaking of the vortex loop as the tail moves along an arc and the vortex is directed downward past the body. The greater vorticity at the tip of the tail is explained by the tail kinematics. Fig. 9Bii shows how, as a result of the tail moving along an arc, the linear velocity at the tip of the tail is greater than that at the tail–body connection. The net result is an axisymmetric flow field.

DISCUSSION

We found that male rusty crayfish (*F. rusticus*) had larger chelae and smaller abdomens than females, but these morphological differences

Journal of Experimental Biology (2020) 223, jeb219873. doi:10.1242/jeb.219873

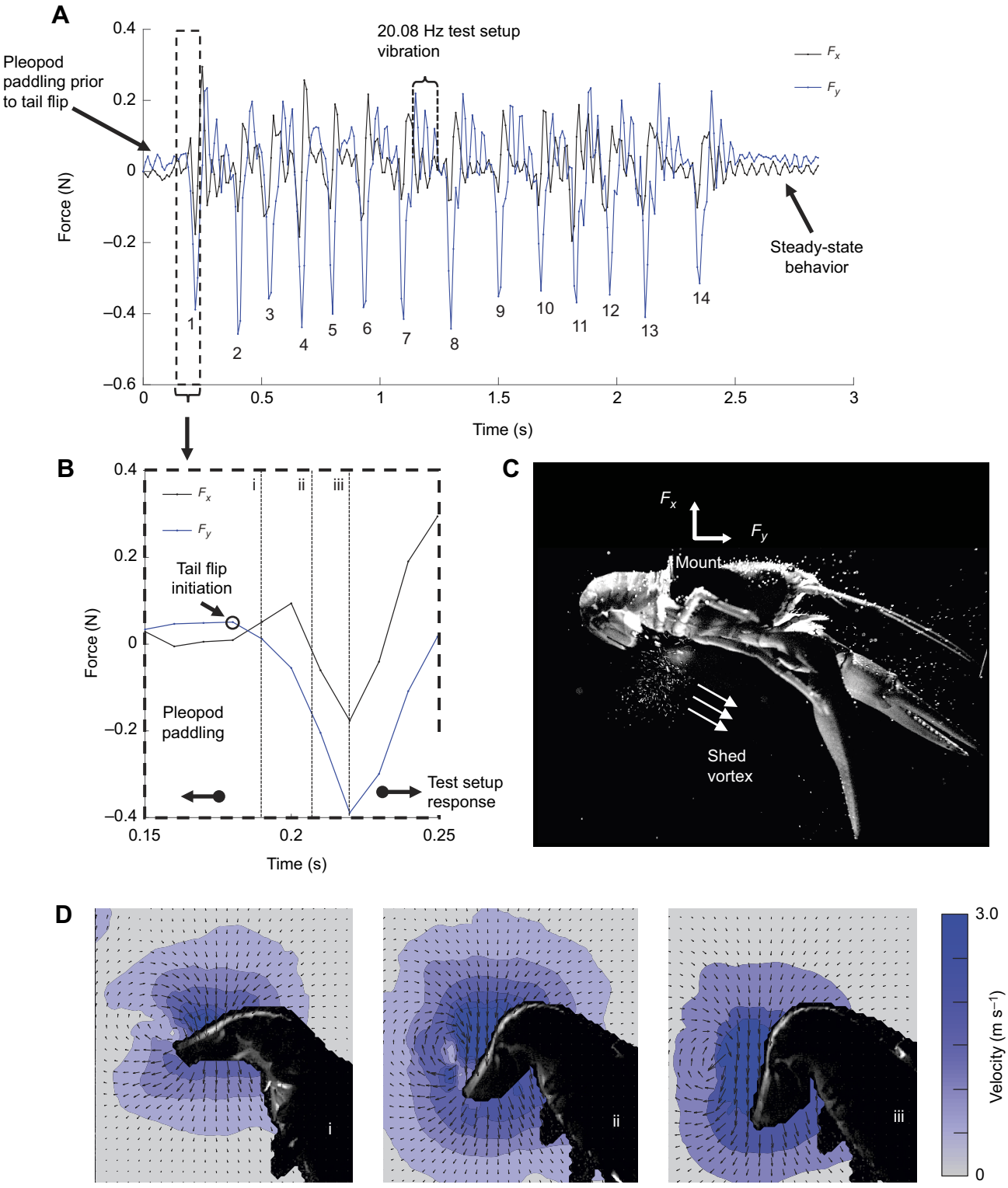

Fig. 7. Force production in rusty crayfish during its tail flip. (A) Force–time histories beginning from steady-state swimming (steady-state movement of pleopods), followed by 14 tail-flip responses. (B) Details of the first flip response. (C) Image showing the trajectory of the vortex that forms at the end of the tail flip. (D) PIV results synchronized with the force–time histories. These plots show that the peak observed in the force–time history corresponds to the instant the crayfish sheds a vortex, which is formed on the outside surface of the tail.

were not associated with significant sex differences in maximum velocity measurements. The lateral portion of the tail fan, the uropods, appeared to be particularly important in the tail-flip escape response, as the length of these structures was correlated with both maximum velocity and maximum force generated during the tail flip. The uropods contributed to the formation of counter-rotational vortices that we observed with particle image velocimetry. Additionally, we showed that the ventral abdominal appendages (pleopods) add

Journal of Experimental Biology (2020) 223, jeb219873. doi:10.1242/jeb.219873

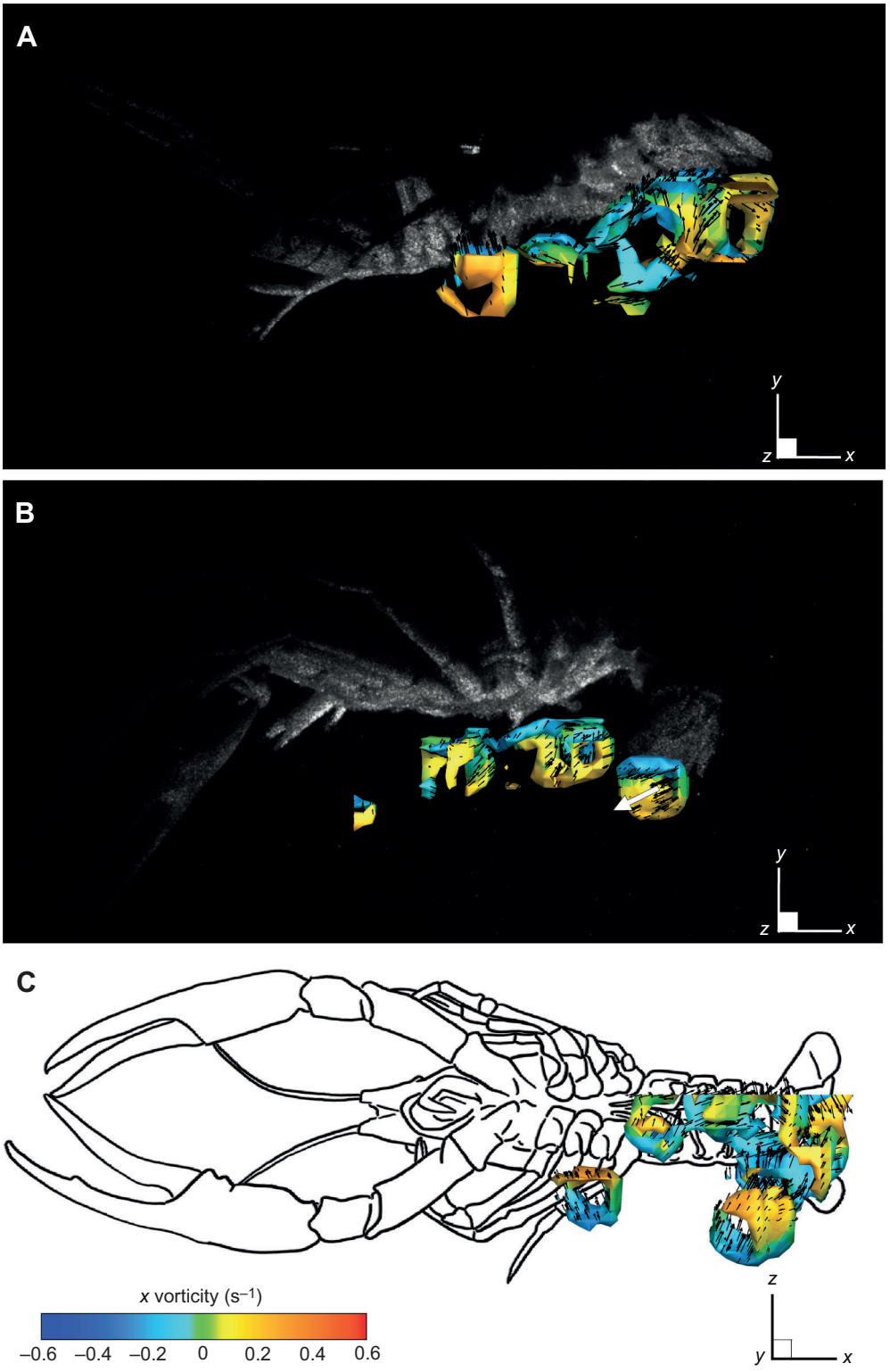

Fig. 8. Volumetric (3D) PIV analyses of flow during crayfish tail-flip behavior. (A) Lateral view of a crayfish immediately before tail flip. The abdomen and tail are extended posteriorly and flow is generated by the pleopods (swimmerets). (B) Lateral view of a crayfish at tail-flip actuation. Thrust generated by the tail vortex to produce rapid backward propulsion is shown with a white vector. (C) Ventral view of the same vortices shown in A to illustrate the lateral position of the anterior-most vortex produced by rapid motion of a walking leg.

momentum by pushing fluid towards the cupped uropods prior to the tail flip. Sexual dimorphism in the velocity of the jet produced by the tail flip, but not in tail vortex vorticity, was observed.

Male crayfish had significantly larger chelae than females. This observation is consistent with previous studies of crayfish (Stein, 1976; Wilson et al., 2009; Wang et al., 2011; Malavé et al., 2018) and with the hypothesis that chelae are under strong sexual selection (Stein, 1976; Sneddon, 1990). Previous studies have reported a negative association between locomotor performance and chelae size, particularly in males (Wilson et al., 2009; Robinson and Gifford, 2019). For example, Wilson et al. (2009) found evidence of a sex-specific trade-off between chelae size and maximum escape velocity in the Australian crayfish *Cherax dispar*. Although we found a significant interaction between chelae width and crayfish sex on escape velocity, this trade-off model performed poorly. Based on AIC values, the trade-off model (AIC=443.64) was

Journal of Experimental Biology (2020) 223, jeb219873. doi:10.1242/jeb.219873

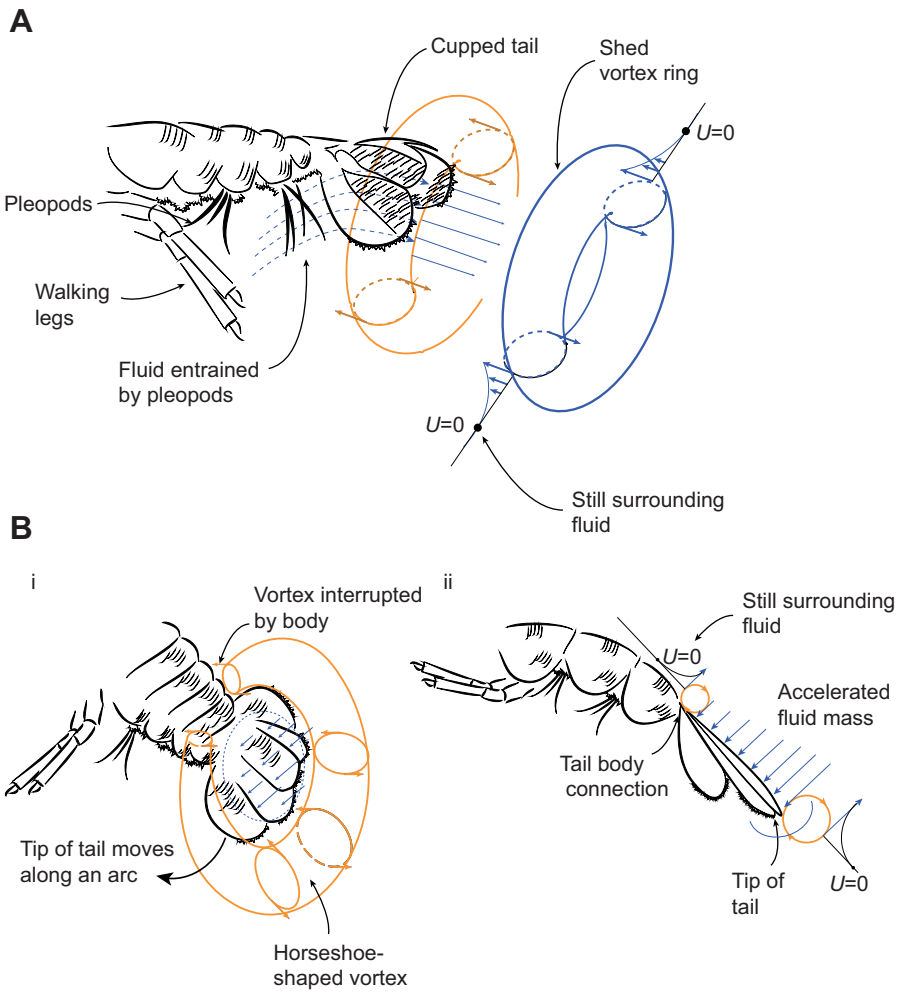

Fig. 9. Hydrodynamic illustrations. (A) Overview of the steady pleopod paddling hydrodynamics. (B) Tail-flip hydrodynamics characterized by (i) a horseshoe-shaped vortex and (ii) an axisymmetic flow created by the rotational trajectory of the tail. *U* refers to the fluid velocity at a specified point in the flow field. In the illustration the water surrounding the specimen is still and therefore has zero velocity, shown as *U*=0 at points relatively far from the crayfish.

outperformed by a multiple regression model including inner uropod length, abdomen length, chelae length and chelae depth (AIC=439.04). Thus, the effect of crayfish morphology on escape velocity was more important than the effect of crayfish sex.

Larger chelae, independent of crayfish sex, had a negative effect on both maximum escape velocity and acceleration during the tail flip. Chelae musculature makes no functional contribution to the tail flip; instead the increased weight and deeper profile of large chelae likely reduce streamlining and increase drag. In a field study of rusty crayfish, Berrill and Arsenault (1984) found that males with large chelae were subject to higher predation rates. There is an extensive literature linking escape velocity and acceleration to predation and fitness in a range of organisms (Irschick and Losos, 1998; Walker et al., 2005; Domenici et al., 2007; Combes et al., 2010).

The crayfish tail fan is composed of a medial telson with two pairs of lateral uropods. Females had longer tails (the combined length of the abdomen and telson) than males (Wang et al., 2011). Females also had significantly wider first and last abdominal segments, similar to what Nauen and Shadwick (1999) found in their study of California spiny lobster *P. interruptus*. Greater abdominal width and tail length may contribute to the production of glair, the mucus used to adhere eggs to the pleopods, and provide a broader surface for brooding eggs (Mason, 1970; Kanciruk, 1980). We found no sex differences in the telson, but females had significantly longer and wider uropods (both the inner and outer pair) than males. To our knowledge, no previous studies have investigated sex differences in crayfish uropods, though greater uropod length was observed in female California spiny lobsters (Nauen and Shadwick, 1999).

The length of the abdomen as well as the width of the first abdominal segment were positively associated with locomotor performance; specifically, escape velocity and acceleration, respectively. Abdominal size can increase acceleration and velocity by accommodating larger extensor and flexor muscles. Nauen and Shadwick (1999) found that both abdomen size and muscle mass scaled isometrically with body mass in the California spiny lobster, suggesting – in that species at least – that larger abdomens have proportionally larger muscle masses. However, Robinson and Gifford (2019) recently found evidence of negative allometry in the flexor muscle mass of Western painted crayfish *Faxonius palmeri longimanus*. Thus, we cannot accurately predict the scaling relationship between abdomen dimensions and tail musculature in rusty crayfish. An area that needs further work is quantifying *in vitro* muscle performance and its relationship to whole-animal performance. For example, Wilson et al. (2009) made *in vitro* preparations of chela muscle in *C. dispar*. They found that male muscles produced more force, but that female muscles had a more rapid twitch rate. If similar differences exist in the abdominal extensor and flexor muscles of rusty crayfish, it would improve our understanding of sex-specific differences in escape performance.

Tail morphology can also impact escape performance by providing more surface area for propulsion. Tail components, such as uropods and flukes, have been shown to be important generators of thrust in

many animal species (Blake, 1981; Webb, 1984; Daniel and Meyhöfer, 1989; Fish et al., 2014; Kikuchi et al., 2014). In our study, the length of the inner uropods was positively related to all metrics of performance (maximum velocity, acceleration and force, the latter through an interaction with sex) suggesting that this morphological feature may play a disproportionately large role in the escape response in crayfish. We speculate that the bulk of the load transfer occurs through the stiffest part of the tail fan (including the inner uropods) and that the more flexible outer uropods (Movies 1 and 3) may be more important for maneuvering.

Male crayfish generally have larger chelae than females, but their escape performance was not significantly different from that of females in our study. However, our hypothesis that male crayfish compensate for the locomotor costs of their sexually selected chelae by enlarging other morphological structures (e.g. Bywater et al., 2018) was not supported. In fact, males had smaller abdomens and shorter uropods than females. The sex-specific relationship between inner uropod length and force production may suggest that males recruit more muscle fibers during the tail flip to overcome the drag imposed by their enlarged chelae, but this hypothesis requires further investigation.

The crayfish tail flip has been a model system in neurobiology for more than 70 years since Wiersma (1947) first described the lateral giant 'command' neurons involved in the escape response in *P. clarkii*. However, an understanding of the fluid dynamics associated with this movement has lagged far behind. The ejection of a jet of water from two closing surfaces can generate substantial 'squeeze forces' and result in locomotion. Jet locomotion is an important locomotor mechanism for many organisms, such as scallops and cephalopods (Trueman and Packard, 1968; Gosline and DeMont, 1985; Cheng and DeMont, 1996), and has been suggested to play an important role in the force production and locomotion of the shrimp *P. danae* (Daniel and Meyhöfer, 1989). By contrast, in the California spiny lobster, maximum forces were achieved prior to the closure of the tail against the cephalothorax, suggesting that jet formation via squeeze forces does not contribute to the force production of the tail-flip escape response (Nauen and Shadwick, 2001). In their study, Nauen and Shadwick (2001) ruled out squeeze forces by comparing force generation with the motion and kinematics of the tail. If squeeze force were responsible for jet formation, the peak force would be expected to occur as the tail closed against the cephalothorax. However, Nauen and Shadwick (2001) observed that maximum force occurred prior to this moment in the California spiny lobster. Similarly, our results demonstrate that the fluid jet produced by the rusty crayfish is not a product of squeeze forces.

Vortical structures were evident in the PIV results and suggest an alternative mechanism for fluid jet formation in crayfish. Both the rapid motion of the anterior walking legs and metachronal paddling of the pleopods generated momentum that was transferred posteriorly and captured by the cupped tail. Pleopods are known to generate a steady jet thrust of the order of 27–54 mN to assist in walking of American lobster (Lim and DeMont, 2009). In addition, crayfish are known to increase pleopod paddling frequency in the presence of fast currents, although the hydrodynamic contribution of pleopods to station holding has not been measured (Maude and Williams, 1983). The cupped shape of the tail during the tail flip likely maximized the retention of momentum generated by the pleopods. It is also possible that tail cupping enhanced thrust generation during the tail flip; cupped fin shape has been shown experimentally to increase positive thrust generation in fishes (Bozkurttas et al., 2008; Esposito et al., 2012).

Conclusions

In this paper we showed that the sexually dimorphic uropods contribute significantly to the performance of the tail-flip escape response of rusty crayfish. Furthermore, the pleopods contribute to the tail flip by pushing fluid towards the uropods. We also provided the first evidence for vortex formation in decapod crustaceans. Future work should employ comparative or manipulative (experimental lengthening or shortening) approaches to further quantify the contribution of uropods and pleopods to crayfish locomotion. Pleopods, for example, are sexually dimorphic and used by females for the brooding of eggs, but the consequences of such differences for escape performance are unknown. Finally, future work should consider how locomotor performance affects predator–prey and competitive interactions. Rusty crayfish are one of several invasive crayfish species that are displacing native crayfish (Garvey et al., 1994). Understanding the relationship between their morphology and escape performance may have implications for biocontrol efforts (Aquiloni et al., 2010).

Acknowledgements

For assistance in the laboratory we thank Haley Amplo, Bridget Benner, Audrey Biondi, Oona Lockyer, Sarah Goodwin, Robert Hamel and Samuel Zhang.

Competing interests

The authors declare no competing or financial interests.

Author contributions

Conceptualization: J.H., T.C., Y.M.-S., B.E.F., E.D.C.; Methodology: J.H., T.C., Y.M.-S., B.E.F., E.D.C.; Validation: T.C., B.E.F.; Formal analysis: J.H., T.C.; Investigation: J.H., T.C., Y.M.-S., B.E.F., E.D.C.; Resources: Y.M.-S., B.E.F., E.D.C.; Writing - original draft: J.H., E.D.C.; Writing - review & editing: J.H., T.C., Y.M.-S., B.E.F., E.D.C.; Visualization: J.H., T.C., Y.M.-S., B.E.F.; Supervision: Y.M.-S., E.D.C.; Funding acquisition: E.D.C.

Funding

This research was funded in part by the Department of Biology at Amherst College.

Data availability

Data are available from the Dryad digital repository (Hunyadi et al., 2020): dryad.cjsxksn3t.

Supplementary information

Supplementary information available online at
https://jeb.biologists.org/lookup/doi/10.1242/jeb.219873.supplemental

References

Aquiloni, L., Buřič, M. and Gherardi, F. (2008). Crayfish females eavesdrop on fighting males before choosing the dominant male. *Curr. Biol.* **18**, R462-R463. doi:10.1016/j.cub.2008.04.006

Aquiloni, L., Brusconi, S., Cecchinelli, E., Tricarico, E., Mazza, G., Paglianti, A. and Gherardi, F. (2010). Biological control of invasive populations of crayfish: the European eel (*Anguilla anguilla*) as a predator of *Procambarus clarkii*. *Biol. Invasions* **12**, 3817-3824. doi:10.1007/s10530-010-9774-z

Arnott, S. A., Neil, D. M. and Ansell, A. D. (1998). Tail-flip mechanism and size-dependent kinematics of escape swimming in the brown shrimp *Crangon crangon*. *J. Exp. Biol.* **201**, 1771-1784.

Berrill, M. and Arsenault, M. (1982). Spring breeding of a northern temperate crayfish, *Orconectes rusticus*. *Can. J. Zool.* **60**, 2641-2645. doi:10.1139/z82-339

Berrill, M. and Arsenault, M. (1984). The breeding behavior of a northern temperate Orconectid crayfish, *Orconectes rusticus*. *Anim. Behav.* **32**, 333-339. doi:10.1016/S0003-3472(84)80265-1

Blake, R. W. (1981). Influence of pectoral fin shape on thrust and drag in labriform locomotion. *J. Zool.* **194**, 53-66. doi:10.1111/j.1469-7998.1981.tb04578.x

Bozkurttas, M., Tangorra, J., Lauder, G. and Mittal, R. (2008). Understanding the hydrodynamics of swimming: from fish fins to flexible propulsors for autonomous underwater vehicles. *Adv. Sci. Technol.* **58**, 193-202. doi:10.4028/www.scientific.net/AST.58.193

Bywater, C. L., Wilson, R. S., Monro, K. and White, C. R. (2018). Legs of male fiddler crabs evolved to compensate for claw exaggeration and enhance claw functionality during waving displays. *Evolution* **72**, 2491-2502. doi:10.1111/evo.13617

Cameron, S. F., Wynn, M. L. and Wilson, R. S. (2013). Sex-specific trade-offs and compensatory mechanisms: bite force and sprint speed pose conflicting demands on the design of geckos (*Hemidactylus frenatus*). *J. Exp. Biol.* **216**, 3781-3789. doi:10.1242/jeb.083063

Cheng, J. Y. and DeMont, M. E. (1996). Jet-propelled swimming in scallops: swimming mechanics and ontogenic scaling. *Can. J. Zool.* **74**, 1734-1748. doi:10.1139/z96-192

Combes, S. A., Crall, J. D. and Mukherjee, S. (2010). Dynamics of animal movement in an ecological context: dragonfly wing damage reduces flight performance and predation success. *Biol. Lett.* **6**, 426-429. doi:10.1098/rsbl.2009.0915

Cromarty, S. I., Cobb, J. S. and Kass-Simon, G. (1991). Behavioral analysis of the escape response in the juvenile lobster *Homarus americanus* over the molt cycle. *J. Exp. Biol.* **158**, 565-581.

Daniel, T. L. and Meyhöfer, E. (1989). Size limits in escape locomotion of Carridean shrimp. *J. Exp. Biol.* **143**, 245-265.

Domenici, P., Turesson, H., Brodersen, J. and Brönmark, C. (2007). Predator-induced morphology enhances escape locomotion in crucian carp. *Proc. Biol. Sci. B* **275**, 195-201. doi:10.1098/rspb.2007.1088

Elner, R. W. and Campbell, A. (1981). Force, function and mechanical advantage in the chelae of the American lobster *Homarus americanus* (Decapoda: Crustacea). *J. Zool.* **193**, 269-286. doi:10.1111/j.1469-7998.1981.tb03444.x

Esposito, C. J., Tangorra, J. L., Flammang, B. E. and Lauder, G. V. (2012). A robotic fish caudal fin: effects of stiffness and motor program on locomotor performance. *J. Exp. Biol.* **215**, 56-67. doi:10.1242/jeb.062711

Fish, F. E., Legac, P., Williams, T. M. and Wei, T. (2014). Measurement of hydrodynamic force generation by swimming dolphins using bubble DPIV. *J. Exp. Biol.* **217**, 252-260. doi:10.1242/jeb.087924

Garvey, J. E., Stein, R. A. and Thomas, H. M. (1994). Assessing how fish predation and interspecific prey competition influence a crayfish assemblage. *Ecology* **75**, 532-547. doi:10.2307/1939556

Gosline, J. M. and DeMont, M. E. (1985). Jet-propelled swimming in squids. *Sci. Am.* **252**, 96-103. doi:10.1038/scientificamerican0185-96

Herberholz, J., McCurdy, C. and Edwards, D. H. (2007). Direct benefits of social dominance in juvenile crayfish. *Biol. Bull.* **213**, 21-27. doi:10.2307/25066615

Hunyadi, J., Currier, T., Modarres-Sadeghi, Y., Flammang, B. E. and Clotfelter, E. D. (2020) Data from Morphology, performance and fluid dynamics of the crayfish escape response. Dryad. doi:10.5061/dryad.cjsxksn3t

Husak, J. F. and Swallow, J. G. (2011). Compensatory traits and the evolution of male ornaments. *Behaviour* **148**, 1-29. doi:10.1163/000579510X541265

Husak, J. F., Ribak, G., Wilkinson, G. S. and Swallow, J. G. (2011). Compensation for exaggerated eye stalks in stalk-eyed flies (Diopsidae). *Funct. Ecol.* **25**, 608-616. doi:10.1111/j.1365-2435.2010.01827.x

Irschick, D. J. and Garland, , Jr., T. (2001). Integrating function and ecology in studies of adaptation: investigations of locomotor capacity as a model system. *Annu. Rev. Ecol. Syst.* **32**, 367-396. doi:10.1146/annurev.ecolsys.32.081501.114048

Irschick, D. J. and Losos, J. B. (1998). A comparative analysis of the ecological significance of maximal locomotor performance in the Caribbean *Anolis* lizards. *Evolution* **52**, 219-226. doi:10.1111/j.1558-5646.1998.tb05155.x

Irschick, D. J., Meyers, J. J., Husak, J. F. and Le Galliard, J. (2008). How does selection operate on whole-organism functional performance capabilities? A review and synthesis. *Evol. Ecol. Res.* **10**, 117-196.

Kanciruk, P. (1980). Ecology of juvenile and adult Palinuridae (spiny lobsters). In *The Biology and Management of Lobsters*, vol. II (ed. J.S. Cobb and B.F. Phillips), pp. 59-96. New York: Academic Press.

Kennedy, D. and Takeda, K. (1965). Reflex control of abdominal flexor muscles in the crayfish: I. the twitch system. *J. Exp. Biol.* **43**, 211-227.

Kikuchi, K., Uehara, Y., Kubota, Y. and Mochizuki, O. (2014). Morphological considerations of fish fin shape on thrust generation. *J. Appl. Fluid. Mech.* **7**, 625-632. doi:10.36884/jafm.7.04.21358

Kojima, W. and Lin, C.-P. (2018). Sprint speed is not reduced by exaggerated male weapons in a flower beetle *Dicronocephalus wallichii*. *Ethology* **125**, 47-56. doi:10.1111/eth.12824

Levinton, J. S. and Judge, M. L. (1993). The relationship of closing force to body size for the major claw of *Uca pugnax* (Decadpoda: Ocypodidae). *Funct. Ecol.* **7**, 339-345. doi:10.2307/2390214

Lim, J. L. and DeMont, M. E. (2009). Kinematics, hydrodynamics, and force production of pleopods suggest jet-assisted walking in the American lobster (*Homarus americanus*). *J. Exp. Biol.* **212**, 2731-2745. doi:10.1242/jeb.026922

Malavé, B. M., Styga, J. M. and Clotfelter, E. D. (2018). Size, shape, and sex-dependent variation in force production by crayfish chelae. *J. Morphol.* **279**, 312-318. doi:10.1002/jmor.20773

Mason, J. C. (1970). Egg-laying in the western North American crayfish, *Pacifasticus trowbridgii* (Stimpson) (Decapoda, Astacidae). *Crustaceana* **19**, 37-44. doi:10.1163/156854070X00608

Maude, S. H. and Williams, D. D. (1983). Behavior of crayfish in water currents: hydrodynamics of eight species with reference to their distribution patterns in southern Ontario. *Can. J. Fish. Aquat. Sci.* **40**, 68-77. doi:10.1139/f83-010

McLean, D. J., Skowron Volponi, M. A. and Tregenza, T. (2018). trajR: An R package for the characterisation of animal trajectories. *Ethology* **124**, 440-448. doi:10.1111/eth.12739

Nauen, J. C. and Shadwick, R. E. (1999). The scaling of acceleratory aquatic locomotion: body size and tail-flip performance of the California spiny lobster *Panulirus interruptus*. *J. Exp. Biol.* **202**, 3181-3193.

Nauen, J. C. and Shadwick, R. E. (2001). The dynamics and scaling of force production during the tail-flip escape response of the California spiny lobster *Panulirus interruptus*. *J. Exp. Biol.* **204**, 1817-1830.

Oufiero, C. E. and Garland, Jr., T. (2007). Evaluating performance of sexually selected traits. *Funct. Ecol.* **21**, 676-689. doi:10.1111/j.1365-2435.2007.01259.x

Robinson, C. D. and Gifford, M. E. (2019). Sexual dimorphism in performance and muscle allocation in the western painted crayfish *Faxonius palmeri longimanus* (Faxon, 1898) (Decapoda: Asticidea: Cambaridae). *J. Crustac. Biol.* **39**, 267-273. doi:10.1093/jcbiol/ruz005

Sneddon, W. A. (1990). Determinants of male mating success in the temperate crayfish *Orconectes rusticus*: chela size and sperm competition. *Behaviour* **115**, 100-113. doi:10.1163/156853990X00301

Stein, R. A. (1976). Sexual dimorphism in crayfish chelae: functional significance linked to reproductive activities. *Can. J. Zool.* **54**, 220-227. doi:10.1139/z76-024

Trueman, E. R. and Packard, A. (1968). Motor performances of some cephalopods. *J. Exp. Biol.* **49**, 495-507.

Tullis, A. and Straube, C. H. T. (2017). The metabolic cost of carrying a sexually selected trait in the male fiddler crab *Uca pugilator*. *J. Exp. Biol.* **220**, 3641-3648. doi:10.1242/jeb.163816

Ueno, R. and Nagayama, T. (2012). Interlocking of chelae is a key factor for dominance hierarchy formation in crayfish. *J. Exp. Biol.* **215**, 2841-2848. doi:10.1242/jeb.072520

Walker, J. A., Ghalambor, C. K., Griset, O. L., McKenney, D. and Reznick, D. N. (2005). Do faster starts increase the probability of evading predators? *Funct. Ecol.* **19**, 808-815. doi:10.1111/j.1365-2435.2005.01033.x

Walter, G. M., van Uitregt, V. O. and Wilson, R. S. (2011). Social control of unreliable signals of strength in male, but not female crayfish, *Cherax destructor*. *J. Exp. Biol.* **214**, 3294-3299. doi:10.1242/jeb.056754

Wang, Q., Yang, J. X., Zhou, G. Q., Zhu, Y. A. and Shan, H. (2011). Length-weight and chelae length-width relationships of the crayfish *Procambarus clarkii* under culture conditions. *J. Freshw. Ecol.* **26**, 287-294. doi:10.1080/02705060.2011.564380

Webb, P. W. (1979). Mechanics of escape responses in crayfish (*Orconectes virilis*). *J. Exp. Biol.* **79**, 245-263.

Webb, P. W. (1984). Form and function in fish swimming. *Sci. Am.* **251**, 72-83. doi:10.1038/scientificamerican0784-72

Wiersma, C. A. G. (1947). Giant nerve fiber system of the crayfish. A contribution to comparative physiology of synapse. *J. Neurophysiol.* **10**, 23-38.

Wilson, R. S., Angilletta, , Jr., M. J., James, R. S., Navas, C. and Seebacher, F. (2007). Dishonest signals of strength in male slender crayfish (*Cherax dispar*) during agonistic encounters. *Am. Nat.* **170**, 284-291. doi:10.1086/519399

Wilson, R. S., James, R. S., Bywater, C. and Seebacher, F. (2009). Costs and benefits of increased weapon size differ between sexes of the slender crayfish, *Cherax dispar*. *J. Exp. Biol.* **212**, 853-858. doi:10.1242/jeb.024547

Wine, J. J. and Krasne, F. B. (1972). The organization of escape behavior in the crayfish. *J. Exp. Biol.* **56**, 1-18.

Yasuda, C., Suzuki, Y. and Wada, S. (2011). Function of the major cheliped in male-male competition in the hermit crab *Pagurus nigrofascia*. *Mar. Biol.* **158**, 2327-2334. doi:10.1007/s00227-011-1736-1